Investigating the Mechanism of Hysteresis Effect in Graphene Electrical Field Device Fabricated on SiO_2 Substrates using Raman Spectroscopy

Hua Xu, Yabin Chen, Jin Zhang, and Haoli Zhang**

The hysteresis effect is a common problem in graphene field-effect transistors (FETs). Usually, the external doping to graphene is considered to be responsible for the hysteresis behavior, but is not yet clearly understood. By monitoring the doping of graphene and the hysteresis in graphene FETs under different atmospheres using in situ Raman spectroscopy, it is confirmed that the electrochemical doping of O_2/H_2O redox couple to graphene is responsible for the hysteresis effect. In addition, Raman spectra of graphene on SiO_2 substrate show stronger doping than that suspended, which indicates that SiO_2 substrate plays an important role in the doping of graphene. Herein it is proposed that the doping species (H_2O and O_2) are bounded at the interface of graphene/SiO_2 substrate by hydrogen-bonds with the silanol groups on SiO_2 substrate. The dynamic equilibrium process of the charge-transfer between H_2O/O_2 redox couple and graphene under electrical field modulation is carefully analyzed using Marcus–Gerischer theory. This work provides a clear view to the mechanism of the hysteresis effect, and is of benefit to a reliable design to suppress the hysteresis in graphene FETs.

1. Introduction

Since its discovery in 2004,[1] graphene, a single-layer of hexagonally arranged carbon atoms, has attracted considerable interest for its application in electrical devices,[2] transparent electrodes,[3] sensors,[4] polymer composites,[5] and catalysis.[6] Among these applications, graphene-based field-effect transistors (FETs) is the most important due to its excellent electrical properties.[7] However, the field-effect characteristic suffers from a stronger hysteresis effect when measured under ambient conditions.[8–11] Moreover, the hysteresis behavior shows dependence on the measurement parameters and the environmental variations.[8,9,12] Therefore, accurate assessment of the electrical transfer properties of graphene is hampered by the presence of the hysteresis effect, which is not desired for graphene FETs. Although the suspended devices,[13] vacuum annealing,[14] and surface passivation[15] can reduce or eliminate the hysteresis, no method can control it in a reproducible fashion due to a lack of understanding of its underlying origin. Therefore, understanding the intrinsic mechanism of the hysteresis effect is important for developing a reliable approach to suppress it.

The mechanism of the hysteresis effect has been studied since the development of carbon-nanotube-based FETs,[16,17] where a similar hysteresis behavior was observed. In general, the charge trapping/detrapping around the graphene is universally recognized as the mechanism of hysteresis effect.[18]

H. Xu, Prof. H. L. Zhang
State Key Laboratory of Applied Organic Chemistry
College of Chemistry and Chemical Engineering
Lanzhou University
Lanzhou 730000, China
E-mail: haoli.zhang@lzu.edu.cn

Y. B. Chen, Prof. J. Zhang
Center for Nanochemistry
Beijing National Laboratory for Molecular Sciences
Key Laboratory for the Physics and Chemistry of Nanodevices
State Key Laboratory for Structural Chemistry of Unstable and Stable Species
College of Chemistry and Molecular Engineering
Peking University
Beijing 100871, China
E-mail: jinzhang@pku.edu.cn

DOI: 10.1002/smll.201102468

For example, the deficiency in the SiO_2 dielectric,[11] silanol groups (Si–OH) present on SiO_2 surface,[19] contamination during fabrication processes[14] as well as adsorbed molecules (H_2O, O_2) from ambient air[11,20,21] are considered to play an important role in the origin of hysteresis effect. Among these views, the prevailing two are charge traps from SiO_2 dielectric and from adsorbed H_2O molecules on devices.[11,22] However, it still remains many questions unclear, for example, the real source of charge traps which produce gate hysteresis in graphene FETs in ambient air; the intrinsic mechanism (or driving force) of the charge trapping/detrapping between charge traps (such as H_2O or O_2 molecules) and graphene; and, the reason that heating treatment typically lead even heavier doping and larger gate hysteresis to the SiO_2 supported graphene devices after re-exposure to air.[23]

As we know, in situ Raman scattering is a nondestructive optical technique which has been used to study the environment and the electrical-field-induced doping to graphene.[21,24] In addition, the relationship between the Raman features and the Fermi level of graphene has been well explained and quantified.[25,26] Here, we present a systematical investigation to the mechanism of hysteresis effect in graphene electrical field device fabricated on SiO_2 substrates by using in situ Raman spectroscopy under different doping atmosphere, as shown in **Figure 1**a. The electrochemical doping of O_2/H_2O redox couple to graphene is confirmed to be responsible for the origin of hysteresis effect. In addition, based on the study to the role of SiO_2 substrate in the doping graphene, we propose that the doping species (H_2O and O_2) are bounded at the interface of graphene/SiO_2 substrate by hydrogen-bond with its surface Si-OH. Finally, the dynamic equilibrium process of the charge-transfer between H_2O/O_2 redox couple and graphene under electrical field modulation is carefully discussed by Marcus–Gerischer (MG) theory.

2. Results and Discussion

2.1. Raman Features and Gate Hysteresis in Graphene Electrical Devices

Figure 1b shows the field-effect characteristics of Raman spectra of graphene in ambient air. The prominent Raman features in graphene are the G band at Γ point (at ~1582 cm^{-1}), and the 2D band (at ~2700 cm^{-1}) involving phonons at the K +ΔK points in the brillouin zone.[24] It can be seen that both G and 2D bands of graphene show the obvious modulations by an electrical field effect. Figure 1c–e reveals how the Raman parameters (the peak position (ω_G) and full-width at half-maximum (FWHM) of G band as well as the intensity ratio of the 2D and G bands (I(2D)/I(G)) vary as a function of gate voltage. The up-shift in ω_G and the decrease in FWHM of G band for both graphene Fermi level moving above (positive gate voltage) and moving down (negative gate voltage) to the Dirac point are in good agreement with the previous report.[25,27] The G peak stiffening is due to the nonadiabatic removal of the Kohn anomaly from the Γ point,[24] and the shift of G band ($\Delta\omega_G$) exhibits a linear relationship to ΔE_F [$\Delta E_F = E_F - E_D$], which is the shift of the Fermi level (E_F) measured from the Dirac point (E_D)] according to the following equation.

$$\hbar\Delta\omega = \frac{\hbar A\left(D_\Gamma^2\right)_F}{\pi M\omega_0(\hbar v F)^2}|\epsilon_F| = \alpha'|\Delta E_F| \quad (1)$$

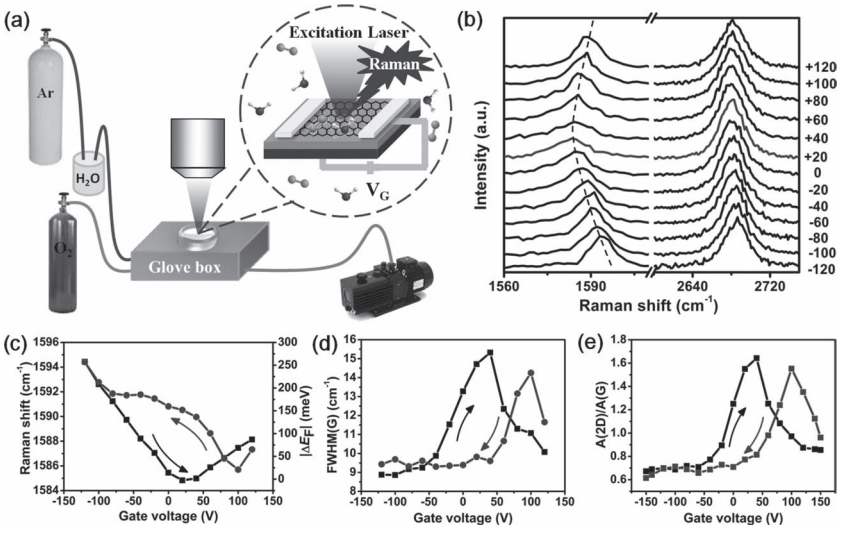

Figure 1. a) Schematic diagram for the in situ monitoring the graphene Fermi level modulation with gate voltage using Raman spectroscopy in different atmosphere. b) Raman spectra of graphene as a function of gate voltage. The gate voltage was reversibly swept between −120 and +120 V, herein we just show the spectra under gate voltage sweeping from −120 to +120 V. The spectra at +20 correspond to the Fermi level at the Dirac point. c) Peak position and d) full-width at half-maxium (FWHM) of the G band as a function of gate voltage. e) Intensity ratio of the G and 2D bands (I(2D)/I(G)) as a function of gate voltage. The curves with arrow indicate the direction of gate voltage sweeping.

Where $\left\langle D_\Gamma^2\right\rangle_F = 45.6\text{eV}^2\text{Å}^{-2}$ is the deformation potential of the E_{2g} mode, M is the atomic weight of carbon, ω_0 is the frequency of the G band in undoped graphene, v_F is the Fermi velocity of graphene, and $\alpha' = 4.39\times10^{-3}$.[26]

From equation (1) we know that the Fermi level was modulated from –0.25 eV to +0.1 eV around the Dirac point under the gate voltage from –120 V to +120 V as seen in Figure 1c. The FWHM sharpening occurs because of the blockage of the decay channel of phonons into electron–hole pairs due to the Pauli Exclusion Principle, when the electron–hole gap becomes higher than the phonon energy. However, the decrease in linewidth saturates when the doping causes a Fermi level shift bigger than half the phonon energy.[25] Similar to the previous report,[24] the intensity ratio of the G and 2D peaks (I(2D)/I(G)) shows an obvious variation as a function of gate voltage. Moreover, the peak position of 2D band shows a relative smaller modulation than that of G band as shown in Figure 1b. Most importantly, we

NANO MICRO small

find that all these Raman features of graphene modulated under reversible gate voltage sweep exhibit a strong hysteresis behavior as presented in Figure 1c–e. We take ω_G as an example to illustrate this hysteresis behavior, the V_{Dirac} (gate voltage corresponding to the charge-neutral point, where ω_G reaches a minimum value) and the curves of ω_G as a function of gate voltage under forward and backward sweeps show shifts and poor reproducibility, respectively, and each curve shows asymmetry between electron and hole doping. This hysteresis behavior in Raman characteristics has been proved to correlate very well with that in electrical transfer characteristics of the FET devices.[28] In fact, the hysteresis effects in both Raman and electrical transfer of graphene FETs reveal the hysteresis of the carrier concentration (or E_F) variation of graphene. Recently, several groups have used electrical transfer to study the doping of graphene.[21] However, the electrical transfer is usually affected by the properties of electrode/channel interface.[29,30] In addition, the V_{Dirac}, which was usually used to quantify the intrinsic doping level of graphene in previous report,[21] is strongly affected by many factors in the measurement. From above discussion, we know that ω_G is a favorable parameter for in situ monitoring the doping-induced Fermi level variation of graphene. In the following study, we focus our attention on the use of ω_G to assess the hysteresis behavior in graphene FETs.

Figure 2a–c shows the curves of ω_G as a function of gate voltage for three different values of gate voltage sweep rate: 40, 20, and 10 V/10s. It can be seen that slower sweep rate results in larger hysteresis behavior. Figure 2c,d shows that large voltage range [–120, 120 V] produces larger gate hysteresis than that for small voltage range [–80, 80 V]. The hysteresis behavior is also affected by the directions of gate voltage sweep as seen in Figure 1c (–120→+120→–120 V) and Figure 2c (+120→–120→+120 V). Furthermore, the V_{Dirac} shows great variations in all these different measurement conditions. Therefore, the hysteresis behavior is dependent on a number of experimental parameters, like the time delay before a sweep started from one end (called hold time, not shown here), range, rate, and direction of the gate voltage sweep, and so on. All these features of hysteresis in the Raman are similar to that in the electrical transfer characteristics which were shown in Figure S2 of the Supporting Information (SI), leading to inaccurate assessment to the performance of the graphene device. Therefore, understanding the intrinsic mechanism of hysteresis effect in graphene FETs is important for rationalizing a design to suppress it.

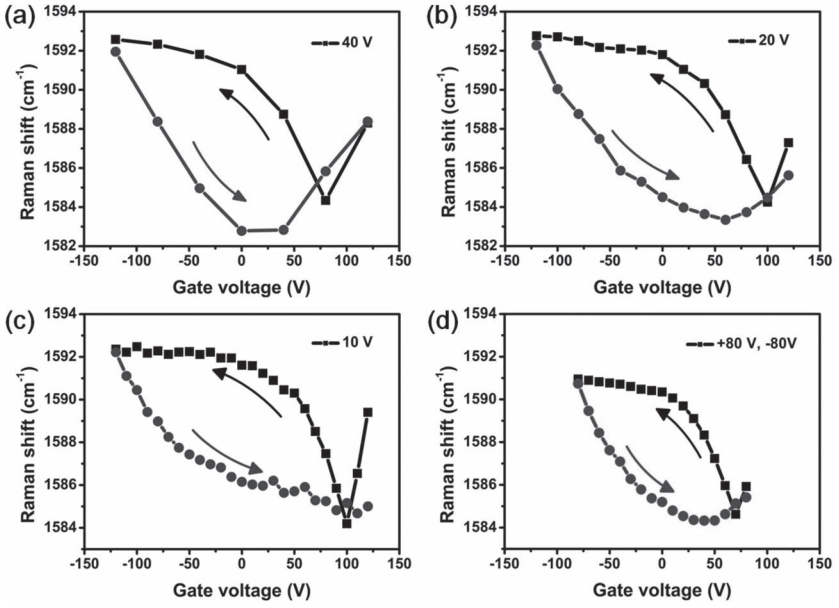

Figure 2. Influencing factors on the gate hysteresis in graphene FETs. The gate voltage is swept from +120 to −120 V, then back to +120 V with sweeping rate: a) 40, b) 20, and c) 10 V/10s. Field-effect characteristic for two different gate voltage sweep ranges: c) [+120, −120] V, d) [+80, −80] V. The gate voltage sweep rate is 10 V/10s.

2.2. Affect of Different Atmosphere on the Doping and Gate Hysteresis in Graphene Devices

In order to explore the origin of hysteresis effect, we treated the samples under conditions of vacuum, vacuum annealing, and exposure to different gas atmosphere. As shown in **Figure 3**a, the hysteresis behavior exhibits an obvious decrease when keeping the sample under 10^{-1} Pa at room temperature for 3 hours compared with that in ambient air. The V_{Dirac} for forward and backward gate voltage sweep moves closer to zero gate voltage. As reported in previous work,[8] a further decrease of the hysteresis and a significant shift of the V_{Dirac} to zero gate voltage can be observed, if continually pumping for a long time (50 hours). This indicates that the doping species, which causes hysteresis and p-doping, are strongly bounded on graphene devices and difficult to be completely desorbed by simple evacuation. Yet, this problem can be improved by annealing the samples in vacuum condition. As shown in Figure 3b, the hysteresis behavior nearly vanishes when annealing the sample at 473 K in vacuum for just about 2 hours. The V_{Dirac} for both forward and backward gate voltage sweep moves to zero gate voltage. However, an even larger doping and gate hysteresis arises when re-exposing the sample into ambient air as shown in Figure 3c. This phenomenon was frequently observed in the electrical transfer characteristics of graphene FETs, but the reason for it remains debated.[14,20,31] Therefore, the nature of the dielectric alone cannot explain why the gate hysteresis in graphene FETs can be tuned using vacuum annealing or air exposure.

To identify the role of O_2 and H_2O (the main composition of air (N_2 and Ar have been proved to be not doped to graphene)) in the doping of graphene and to explore the origin of hysteresis effect in graphene FETs, the samples were exposed to O_2, H_2O and $O_2 + H_2O$ atmosphere with controlled dose, respectively. As shown in Figure 3d–f, exposing the samples to O_2 or

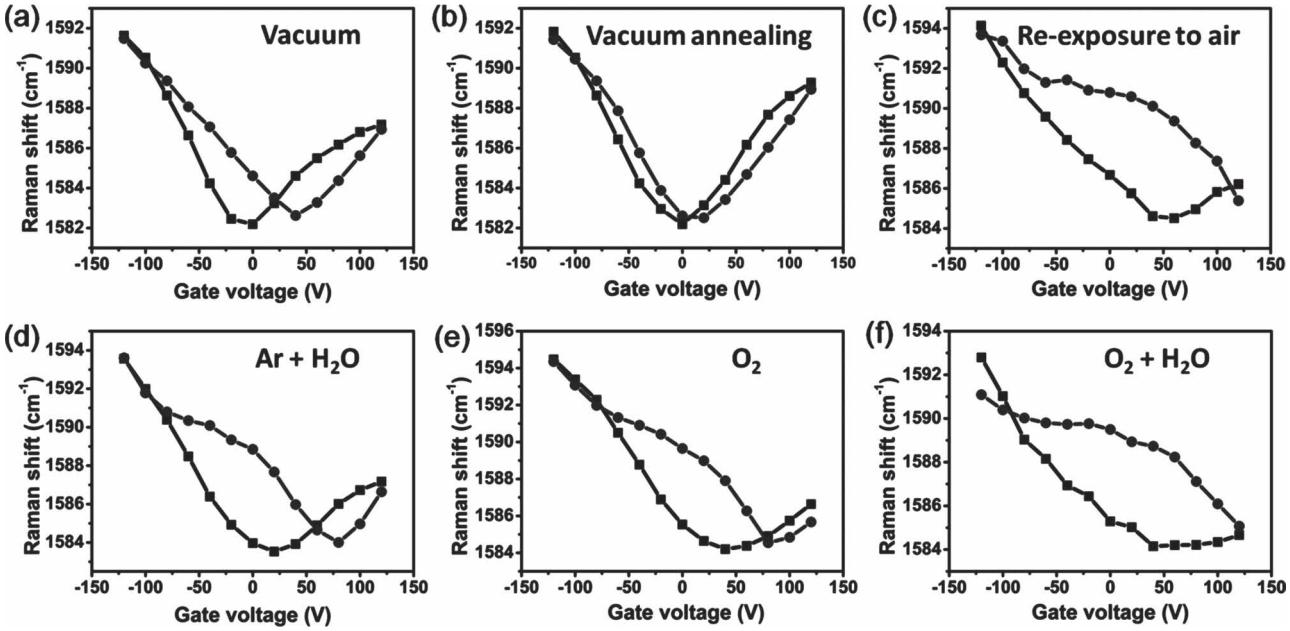

Figure 3. Field-effect characteristic of Raman spectra of graphene under different atmosphere treatments: a) in vacuum (10^{-1} Pa) for 3 h, b) annealing in vacuum for 2 h, c) re-exposure to air after vacuum annealing, d) Ar-containing water vapor (200 Pa, ~50% relative humidity), e) O_2 (100 Pa), and f) O_2-containing water vapor (100 Pa, ~50% relative humidity).

H_2O atmosphere after vacuum treatment for 3 hours induced a slight p-doping (V_{Dirac} moved to positive gate voltage) and a small gate hysteresis in graphene FETs. While exposing it to the mixture of O_2 and H_2O brings a heavier doping and a larger gate hysteresis than that exposed to O_2 or H_2O alone. In fact, previous work has also shown a similar phenomena that there is nearly no doping when exposing the samples to O_2 or H_2O alone, while a larger doping arises when espoused to the mixture of O_2 and H_2O.[20,21] The smaller doping and gate hysteresis of graphene exposure to O_2 or H_2O alone in our results should be due the affect of the residue O_2 or H_2O, which is difficult to be completely eliminated in our experiment conditions. In spite of this, we can find a larger gate hysteresis in the mixture of O_2 and H_2O than that in O_2 and H_2O alone in a same partial pressure. So, we can make sure that the combination of O_2 and H_2O plays a key role in the doping of graphene and the origin of hysteresis effect.

2.3. Role of SiO_2 Substrate in the Doping of Graphene, and Electrochemical Doping Mechanism of Graphene

Now, we assess the molecular species (H_2O and O_2) with what kind of role forms to produce the gate hysteresis. There are two basic questions which need to be answered. One is the form of molecular species interacting with graphene and the role of SiO_2 substrate in the doping of graphene; another is the intrinsic mechanism (driving force) of the charge-transfer between graphene and molecular species. For the former question, we examined the doping of freshly prepared graphene under different atmosphere by Raman spectra as shown in **Figure 4**a. In this case, the bottom and top surface of graphene are just contact with the SiO_2 substrate and atmosphere, respectively, which can avoid the potential effect of the resists (PMMA residues in the device preparation) on the experiment results. Graphene deposited on a freshly cleared SiO_2/Si substrate exhibits a smaller p-doping, but a larger p-doping arises when exposing the samples in ambient air for one day (step i in Figure 4a). The p-doping can be eliminated by exposing the samples in vacuum for about 3 hours (step ii). Similar to above results, introducing the mixture of H_2O and O_2 (step v in Figure 4a) brings a larger doping than that for introducing O_2 alone (step iii in Figure 4a). In addition, it is need to be noted that the doping becomes more difficult to be recovered by evacuation (step vi in Figure 4a) after introducing H_2O than that for introducing O_2 alone (step iv in Figure 4a). So, simple attributing the p-doping of graphene in ambient air to the adsorption of H_2O and O_2 on the surface of graphene may not be accurate, as theory and experiment have indicated that graphene is very hydrophobic.[10,32] Much work has considered that SiO_2 substrates plays an important role in the doping of graphene in ambient air.[19,20] To explore the role of SiO_2 substrate, we compared the doping of graphene on SiO_2 substrate with that suspended on a trench. As shown in Figure 4b, the ω_G of graphene on SiO_2 substrate shows an up-shift of about 3 cm^{-1} after introducing O_2/H_2O species, while that for the freestanding region is essentially unchanged. This result indicates that doping does not occur for the freestanding graphene, which is consistent with the substrate effects in carbon nanotubes and graphene.[13,33] Therefore, we are inclined to the view that H_2O and O_2 molecular species exist at the interface between graphene and SiO_2 substrate other than adsorbed on the surface of graphene.

As we know, a layer of Si-OH usually exists on the surface of SiO_2 substrate, especially after the substrate was washed

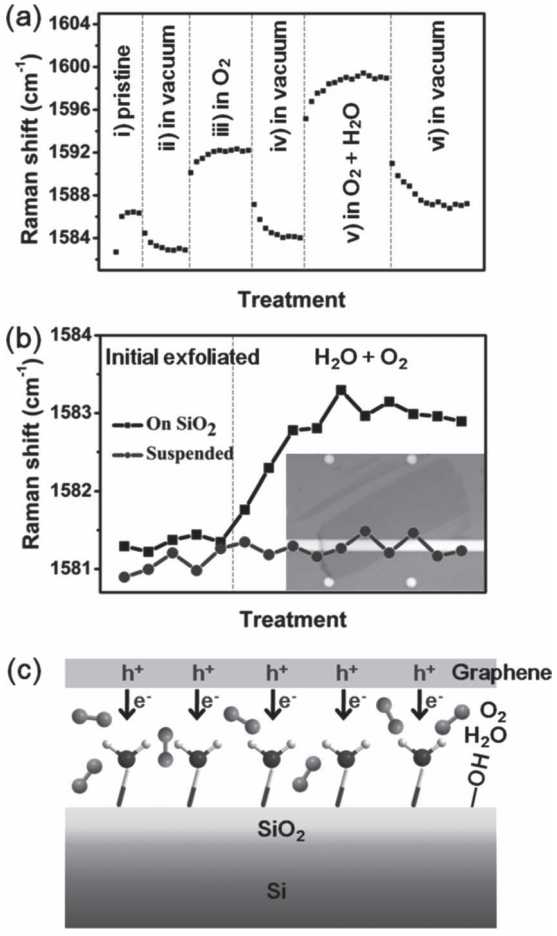

Figure 4. a) Atmosphere sensitivity of initial exfoliated graphene on SiO_2 substrate. The doping-induced Fermi level variation in (i) ambient air, (ii) vacuum (10^{-1} Pa), (iii) O_2, (iv) vacuum (10^{-1} Pa), (v) O_2-containing water vapor (10^5 Pa, ~50% relative humidity) and (vi) vacuum (10^{-1} Pa) conditions were monitored by Raman G band energy. b) Comparison of the doping of initial exfoliated graphene (trilayers) supported on SiO_2 substrate and suspended on trench by exposing the samples to O_2-containing water vapor (10^5 Pa, ~50% relative humidity). c) Schematic depicting the p-doping of SiO_2 substrate supported graphene in ambient air.

by piranha solution or plasma cleaner. Then, doping species (H_2O and O_2 molecules) are easily bounded on the SiO_2 substrate by hydrogen band with Si-OH when exposing it to ambient air. Kelvin probe microscopy and X-ray spectroscopy have shown that four or five water layers exist on the surface of SiO_2 films grown on Si.[34] Based on above discussions, we propose that the doping species (H_2O and O_2) are bonded at the interface of graphene/SiO_2 substrate by hydrogen-bonding with its surface Si-OH as shown in Figure 4c. This understanding provides a basis for understanding many behaviors which were widely discussed in previous reports for graphene supported on SiO_2 substrate. First, the initial exfoliated graphene should be in simple loose contact with the rough SiO_2 substrate (height variation about 1 nm), which brings a relative smaller doping because the charge-transfer requires that doping species be close enough to exchange electrons with graphene. This is also the reason for the doping state of initially exfoliated graphene showing a wide variety in different samples and a local microscopic charge inhomogeneity previously reported for graphene on SiO_2 substrate.[20,35] Second, a monolayer or sub-monolayer of hydrogen-bonded H_2O and O_2 remain on the SiO_2 substrate and cannot be removed by simple evacuation at room temperature due to the strong hydrogen-bond. This is responsible for the residual doping and hysteresis observed in graphene FETs after longtime vacuum treatment. Nevertheless, these bounded H_2O and O_2 species can be easily removed by heating treatment in the vacuum condition at 473 K. At the same time, thermal annealing leads graphene to closely couple to the SiO_2 substrate as previous report,[20] then the doping species are re-bounded on SiO_2 substrate after re-exposure to air. So, an even larger doping and hysteresis behavior arise in graphene FETs after vacuum annealing and re-exposure to air.

For the latter question, we should understand what the drive force of the charge-transfer between graphene and molecular species and their dynamic process are. We know, the electron affinity of O_2 (0.44 eV) is much lower than the E_F of graphene (4.6 eV), direct charge-transfer between them is unfavorable. As our results demonstrated, an O_2/H_2O layer should be present at the interface of graphene/SiO_2 substrate in order to induce p-doping and gate hysteresis in graphene FETs. This implies that electrons are not simply trapped by H_2O, O_2 or Si-OH as reported before.[11,19] Our results support a mechanism that electrons are transferred from graphene to H_2O/O_2 redox couple through an electrochemical redox reaction. This conclusion is based on a recent study by Chakrapani et al.,[36] where they found that the p-doping of diamond in ambient air is due to the electron transfer from the diamond to the H_2O/O_2 redox couple. In addition, recent theoretical calculation has shown that there should be two types of dopants for graphene.[37] The first one called electronic doping occurs via a direct exchange of electrons between adsorbate and graphene, which will not lead to hysteresis effects. The second one called electrochemical doping occurs via redox reactions involving H_2O/O_2 and graphene, which will lead to hysteresis effects.

The electrons spontaneously transfer between graphene and H_2O/O_2 redox couple through the electrochemical redox reaction:

$$O_2 + 2H_2O + 4e^- \text{ (graphene)} = 4OH^- \quad (2)$$

Here, the electrochemical potential of the redox couple in the atmospheric, calculated from Nernst equation, is about –5.3 eV.[36,37] Marcus–Gerischer (MG) theory was used to explain the doping mechanism of graphene and the dynamic process of charge-transfer in graphene FETs. MG theory is a universal theory in electrochemistry, which has been widely used to describe the charge-transfer in electrochemical reactions between metal and redox system.[38,39] As shown in **Figure 5**a, the electronic density of states (DOS) function, which reflects the electron energy level distribution around oxidation potential (E_{ox}) and reduction potential (E_{red}), for occupied and un-occupied states are defined as D_{ox} and D_{red}, respectively. The Fermi level of the solution E_{redox} is the energy where the DOS of reducing and oxidizing species are equal: $D_{ox}(E_{redox}) = D_{red}(E_{redox})$.[21] For charge-transfer

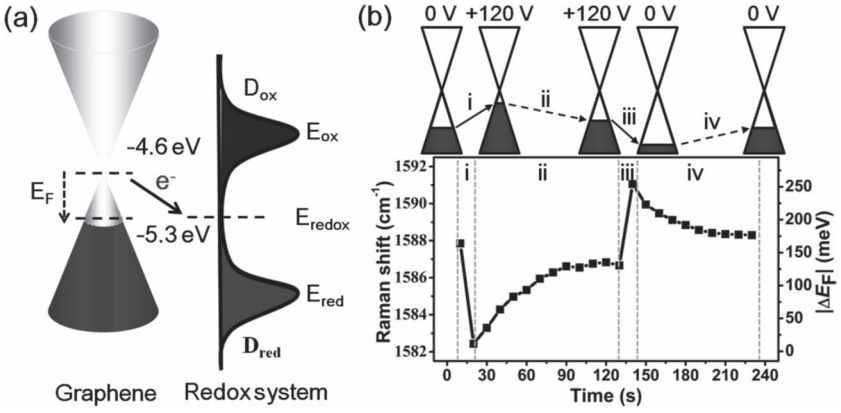

Figure 5. a) Doping mechanism of graphene depicted by Marcus–Gerischer theory. The arrow indicates the direction of charge-transfer. b) Time evolution of ω_G and Fermi level of graphene after the equilibrium of charge-transfer between molecular species and graphene was broken by changing the gate voltage. The gate voltage applied to graphene device steps from (i) 0 to +120 V, (ii) holding at +120 V for about 100 s, (iii) step from +120 to 0 V, and (iv) keeping at 0 V for about 100 s.

occuring, the Fermi function of metal should match with the DOS of redox couple according to MG theory. So, the Fermi level of graphene (-4.6 eV) lies above the electrochemical potential of the O_2/H_2O redox couple (–5.3 eV) providing a strong driving force for electrons transfer from the Fermi level of graphene to the unoccupied state of O_2/H_2O redox couple.

2.4. Dynamic Equilibrium of Charge-Transfer Process Between O_2/H_2O Redox Couple and Graphene Under the Electrical Field Modulation

The dynamic equilibrium and the rate of charge-transfer between O_2/H_2O redox couple and graphene under electrical field modulation are also well described through this simple MG model. According to MG theory, the direction and the rate of charge-transfer (the rate of electron transfer from graphene to solution species and from solution species to graphene are represented by $R_{G\text{-}M}$ and $R_{M\text{-}G}$, respectively) are proportional to the overlap integral of the E_F of graphene and the DOS of molecule species.

$$R_{G-M} \propto (\text{overlap of } E_F \text{ and } D_{ox})$$

$$R_{M-G} \propto (\text{overlap of } E_F \text{ and } D_{red})$$

Figure 5b presents the time evolution of ω_G (or E_F) of graphene after the equilibrium of charge-transfer between molecular species and graphene was broken by changing the gate voltage. At zero gate voltage, the ω_G of graphene is at 1588 cm^{-1} which shows an up-shift compared with the intrinsic one (at 1582 cm^{-1}) due to the doping-induced E_F down-shift by O_2/H_2O redox couple. We assume that the charge-transfer between graphene and O_2/H_2O redox couple reaches equilibrium at zero gate voltage, where E_F and E_{redox} are equal as shown in the middle of Figure S3b of the SI. According to MG theory, this equilibrium can be broken by the electrical-field-induced graphene E_F variation. When apply a +120 V gate voltage (step i in Figure 5b) to graphene, the ω_G decreases to about 1582 cm^{-1} with the E_F up-shifting, which leads the overlap integral of E_F and D_{ox} to be larger than that of E_F and D_{red} as shown in the right of Figure S3b of the SI. Then, the reaction 2 proceeds to the forward direction, that means the electrons transfer from graphene to molecule species. So, the ω_G (E_F) cannot hold at its position, while it gradually increases (decreases) until a new equilibrium is produced as the time increases (step ii in Figure 5b). When step the gate voltage from positive to zero (step iii in Figure 5b), the electron concentration of graphene contributed by the gate voltage immediately vanishes, while graphene has lost more electrons to molecule species than that at original zero gate voltage in the period of positive gate voltage (step ii in Figure 5b). In this case, the ω_G up-shifts even higher (E_F down-shifts even lower) than that at the original zero gate voltage (step iii in Figure 5b). In addition, this step leads the overlap integral of E_F and D_{red} to be larger than that of E_F and D_{ox}, which causes a break to the charge-transfer equilibrium again. Then, the reaction 2 proceeds to the backward direction, that means the electrons transfer from molecule species to graphene. So, the ω_G (E_F) gradually decreases (increases) until a new equilibrium is produced as the time increases (step iv in Figure 5b). The time evolution of ω_G (or E_F) for applying a negative gate voltage shows a similar variation trend as that for positive gate voltage as shown in Figure S3a of the SI.

In addition, it needs to be noted that the time for the charge-transfer from nonequilibrium to equilibrium needs about 100 s which are in the same order of magnitude with that reported by Liu et al.,[22] but far shorter than that reported by Martel et al.[21] At present, there are really many problems in the accurately quantify the charge-transfer rate due to a lack of appropriate quantitative parameter and approach, which is detailed illustrated in the SI. Here, we believe that using the quantitative relationship between ω_G and E_F to in situ monitoring the doping of graphene is an appropriate for the study of charge-transfer rate. As we have demonstrated above, we consider that the charge-transfer rate is related to the reaction kinetics of reaction 2. The charge-transfer rate is proportional to the overlap integral of E_F of graphene and D_{ox}/D_{red} of the molecule species. This means that the $R_{G\text{-}S}$ decreases nonlinearly with time increasing after applying a positive gate voltage due to the decreases of the overlap integral of E_F and D_{ox} as the E_F down-shifts. So, the Fermi level (carrier concentration) exhibits a nonlinear variation with time increasing after disturbing the equilibrium of reaction by changing the stress gate voltage as shown in step ii and step iv of Figure 5b. Corresponding electrical measurement also confirms our conclusions as show in Figure S4.

From above discussion, we know that there is a complex dynamic equilibrium process in the charge-transfer between graphene and molecule species in graphene FETs. The

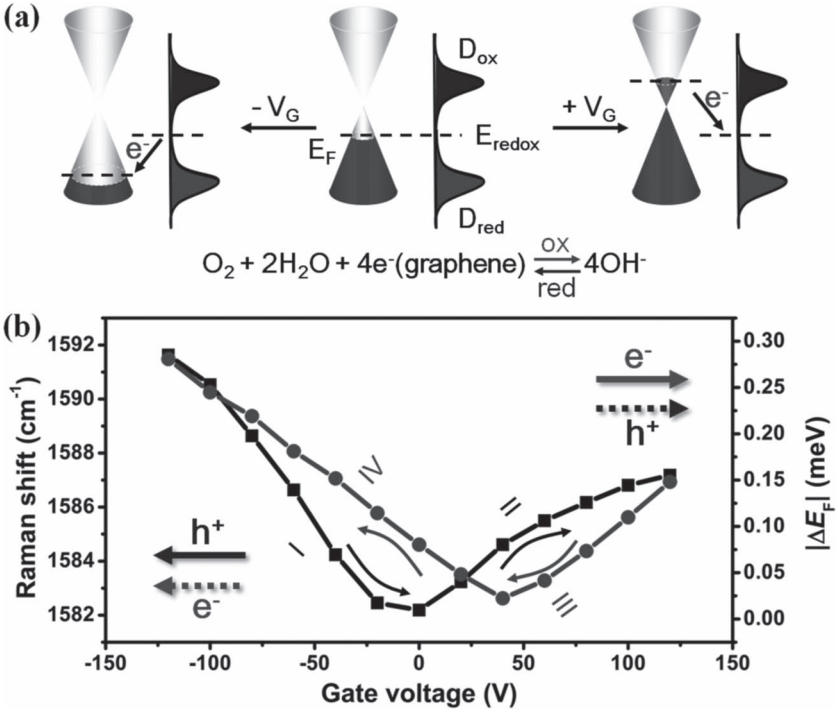

Figure 6. a) Schematic illustration to the dynamic equilibrium process of charge-transfer between molecule species and graphene through the redox reaction under different gate voltages. b) The hysteresis process of hysteresis effect in graphene FETs. The solid and the dot arrows in (b) represent the contribution of the gate voltage and the molecule species to the E_F of graphene (the arrows represent two contributions of E_F: electron and hole), respectively. And, the curves with arrows indicate the direction of gate voltage sweeping, which helps us to distinguish the difference of hysteresis behavior in electron and hole doping side.

direction and the rate of charge-transfer continuously change as the E_F of graphene up-shifts and down-shifts under the reversible gate voltage modulation. Here, we define the contribution of gate voltage and molecule species induced doping to the E_F (or carrier concentration) variation of graphene as E_{FG} and E_{FM}, respectively. The electrical field characteristic in graphene FETs can be simply divided into four processes as presented in **Figure 6**b. Process I, E_{FG} up-shifts with an even speed, and E_{FM} up-shifts with a decreasing speed due to the $R_{M\text{-}G}$ decreasing with the overlap integral of E_F and D_{red} decreasing (see the left of Figure 6a), thus E_F up-shifts rapidly; Process II, E_{FG} up-shifts with an even speed, but E_{FM} down-shifts with an increasing speed due to the $R_{G\text{-}M}$ increasing with the overlap integral of E_F and D_{ox} increasing (see the right of Figure 6a), thus E_F up-shifts slowly; Process III, E_{FG} down-shifts with an even speed, and E_{FM} down-shifts with a decreasing speed due to the $R_{G\text{-}M}$ decreasing with the overlap integral E_F and D_{ox} decreasing (see the right of Figure 6a), thus E_F down-shifts rapidly; Process IV, E_{FG} down-shifts with an even speed, but E_{FM} up-shifts with an increasing speed due to the $R_{M\text{-}G}$ increasing with the overlap integral E_F and D_{red} increasing (see the left of Figure 6a), thus E_F down-shifts slowly. So, the hysteresis behavior shows clockwise on the electron doping side and counterclockwise on the hole doping side, which is the main feature of hysteresis effect in graphene FETs in ambient.[22] This is the first time we concretely describe the hysteresis process in graphene FETs from its behind chemistry. According to such an analysis to the hysteresis process, we can readily understand many phenomena in electrical characteristic of graphene FETs, for example, the un-superposition between forward and backward gate voltage sweep and the asymmetry between electron and hole transport. In addition, our experiment results also confirmed the theory expectation about the relationship between these two types of dopants for graphene and the hysteresis effect in grephene FETs (see the SI for a more detailed discussion).

3. Conclusion

In summary, by studying the doping of graphene in different atmosphere treatments using in situ Raman spectroscopy, we present a clear picture of the mechanism of the hysteresis effect in graphene FETs and show that the charge-trapping/-detrapping between graphene and O_2/H_2O redox couple at the interface of graphene/SiO_2 substrate is responsible for the origin of the hysteresis effect. MG theory was used to explain the charge-transfer mechanism of O_2/H_2O redox couple to graphene and to analyze their dynamic equilibrium process under the electrical field modulation. Based on MG theory, the electrical field characteristic in graphene FETs was simply divided into four processes, which helps us to more clearly look into the origin of the hysteresis effect. In addition, we propose that the doping species (H_2O and O_2), which causes gate hysteresis in graphene FETs, are bounded at the interface of graphene/SiO_2 substrate by hydrogen-bonding with its surface Si–OH. This view can well explain many phenomena for SiO_2-substrate-supported graphene. The mechanism of the hysteresis effect in graphene FETs is also applicable to that in carbon nanotube FETs. Building on this understanding, investigations into using rational design to suppress the hysteresis effect in graphene FETs are ongoing.

4. Experimental Section

Preparation of Graphene Device: Graphene devices were fabricated as described in our previous work.[27] Briefly, graphene sheets were prepared by mechanical exfoliation of Kish graphite using scotch tape and then deposited onto Si substrate with a 300 nm oxide layer. Monolayer graphene were identified with the help of optical microscopy (OM) and Raman spectroscopy. Standard electron beam lithography and lift-off techniques were finally used to fabricate the contact electrodes to the graphene. The electrodes were made of Cr/Au (5 nm/50 nm). The OM image of the typical graphene device is shown in Figure S1a of the SI.

Raman Measurement and Controlled Atmosphere Experiments: Raman spectra were obtained by using a Horiba HR800 Raman

system with a 600 lines/mm grating and a 514.5 nm laser. The incident laser beam was focused by a 50× objective and the laser power on the samples was kept below 0.5 mW to avoid laser-induced heating. The spectra integration time was 10 s per spectrum. The intensities and frequencies of the peaks were obtained by fitting them with a Lorentzian function. For annealing, vacuum and controlled atmosphere experiments, a homemade vacuum probe station was used. The pressure could be down to 10^{-1} Pa in the vacuum probe station by pumping for about 1 minute. The temperature can be up to 473 K with a heating stage.

Supporting Information

Supporting Information is available from the Wiley Online Library or from the author.

Acknowledgements

This work was supported by MOST (2006CB932701, 2006CB932403, 2007CB936203), NSFC (10774006, 50972001, 20725307 and 50821061), "The Fundamental Research Funds for the Central Universities".

[1] K. S. Novoselov, A. K. Geim, S. V. Morozov, D. Jiang, Y. Zhang, S. V. Dubonos, I. V. Grigorieva, A. A. Firsov, *Science* **2004**, *306*, 666.
[2] A. K. Geim, K. S. Novoselov, *Nat. Mater.* **2007**, *6*, 183.
[3] G. Eda, G. Fanchini, M. Chhowalla, *Nat. Nanotechnol.* **2008**, *3*, 270.
[4] F. Schedin, A. K. Geim, S. V. Morozov, E. W. Hill, P. Blake, M. I. Katsnelson, K. S. Novoselov, *Nat. Mater.* **2007**, *6*, 652.
[5] D. A. Dikin, S. Stankovich, E. J. Zimney, R. D. Piner, G. H. B. Dommett, G. Evmenenko, S. T. Nguyen, R. S. Ruoff, *Nature* **2007**, *448*, 457.
[6] P. V. Kamat, *J. Phys. Chem. Lett.* **2010**, *1*, 520.
[7] C. Stampfer, E. Schurtenberger, F. Molitor, J. G. ttinger, T. Ihn, K. Ensslin, *Nano Lett.* **2008**, *8*, 2378.
[8] T. Lohmann, K. v. Klitzing, J. H. Smet, *Nano Lett.* **2009**, *9*, 1973.
[9] H. Xu, Y. B. Chen, W. G. Xu, H. L. Zhang, J. Kong, M. S. Dresselhaus, J. Zhang, *Small* **2011**, *7*, 2945.
[10] X. Q. Zhang, S. H. Wan, J. B. Pu, L. P. Wang, X. Q. Liu, *J. Mater. Chem.* **2011**, *21*, 12251.
[11] M. Lafkioti, B. Krauss, T. Lohmann, U. Zschieschang, Hagen Klauk, K. v. Klitzing, J. H. Smet, *Nano Lett.* **2010**, *10*, 1149.
[12] H. Wang, Y. H. Wu, C. X. Cong, Jing Zhi Shang, T. Yu, *ACS Nano* **2010**, *4*, 7221.
[13] M. Muoth, T. Helbling, L. Durrer, S. W. Lee, C. Roman, C. Hierold, *Nat. Nanotechnol.* **2010**, *5*, 589.
[14] Z. G. Cheng, Q. Y. Zhou, C. X. Wang, Q. Li, C. Wang, Y. Fang, *Nano Lett.* **2011**, *11*, 767.
[15] S. A. McGill, S. G. Rao, P. Manandhar, P. Xiong, *Appl. Phys. Lett.* **2006**, *89*, 163123.
[16] W. Kim, A. Javey, O. Vermesh, Q. Wang, Y. M. Li, H. J. Dai, *Nano Lett.* **2003**, *3*, 193.
[17] J. S. Lee, S. Ryu, K. Yoo, I. S. Choi, W. S. Yun, J. Kim, *J. Phys. Chem. C* **2007**, *111*, 12504.
[18] A. Vijayaraghavan, S. Kar, C. Soldano, S. Talapatra, O. Nalamasu, P. M. Ajayan, *Appl. Phys. Lett.* **2006**, *89*, 162108.
[19] P. Joshi, H. E. Romero, A. T. Neal, V. K. Toutam1, S. A. Tadigadapa, *J. Phys.: Condens. Matter* **2010**, *22*, 334214.
[20] S. Ryu, L. Liu, S. Berciaud, Y. J. Yu, H. Liu, P. Kim, G. W. Flynn, L. E. Brus, *Nano Lett.* **2010**, *10*, 4944.
[21] P. L. Levesque, S. S. Sabri, C. M. Aguirre, J. Guillemette, M. Siaj, P. Desjardins, T. Szkopek, R. Martel, *Nano Lett.* **2011**, 132.
[22] Z. h. Liu, A. A. Bol, W. Haensch, *Nano Lett.* **2011**, *11*, 523.
[23] C. R. Dean, A. F. Young, I. Meric, C. Lee, L. Wang, S. Sorgenfrei, K. Watanabe, T. Taniguchi, P. Kim, K. L. Shepard, J. Hone, *Nat. Nanotechnol.* **2010**, *5*, 722.
[24] A. Das, S. Pisana, B. Chakraborty, S. Piscanec, S. K. Saha, U. V. Waghmare, K. S. Novoselov, H. R. Krishnamurity, A. K. Geim, A. C. Ferrari, A. K. Sood, *Nat. Nanotechnol.* **2008**, *3*, 210.
[25] J. Yan, Y. B. Zhang, P. Kim, A. Pinczuk, *Phys. Rev. Lett.* **2007**, *98*, 166802.
[26] S. Pisana, M. Lazzeri, C. Casiraghi, K. S. Novoselov, A. K. Geim, A. C. Ferrari, F. Mauri, *Nat. Mater.* **2007**, *6*, 198.
[27] H. Xu, L. M. Xie, H. L. Zhang, J. Zhang, *ACS Nano* **2011**, *5*, 5338.
[28] S. Yuan, Q. Zhang, Y. You, Z.-X. Shen, D. Shimamoto, M. Endo, *Nano Lett.* **2009**, *9*, 383.
[29] B. Huard, N. Stander, J. A. Sulpizio, D. Goldhaber-Gordon, *Phys. Rev. B* **2008**, *78*, 121402(R).
[30] D. B. Farmer, R. Golizadeh-Mojarad, V. Perebeinos, Y. M. Lin, G. S. Tulevski, J. C. Tsang, P. Avouris, *Nano Lett.* **2009**, *9*, 388.
[31] C. C. Chen, W. Bao, J. Theiss, C. Dames, C. N. Lau, S. B. Cronin, *Nano Lett.* **2009**, *9*, 4172.
[32] O. Leenaerts, B. Partoens, F. M. Peeters, *Phys. Rev. B* **2009**, *79*, 235440.
[33] S. Berciaud, S. Ryu, L. E. Brus, T. F. Heinz, *Nano Lett.* **2009**, *9*, 346.
[34] A. Verdaguer, C. Weis, G. Oncins, G. Ketteler, H. Bluhm, M. Salmeron, *Langmuir* **2007**, *23*, *9699*.
[35] J. Xue, J. Sanchez-Yamagishi, D. Bulmash, P. Jacquod, A. Deshpande, K.Watanabe, T. Taniguchi, P. Jarillo-Herrero, B. J. LeRoy, *Nano Lett.* **2011**, *11*,
[36] V. Chakrapani, J. C. Angus, A. B. Anderson, S. D. Wolter, B. R. Stoner, G. U. Sumanasekera, *Science* **2007**, *318*, 1424.
[37] H. Pinto, R. Jones, J. P. Goss, P. R. Briddon, *Phys. Status Solidi A* **2010**, *207*, 2131.
[38] J. O. M. Bockris, S. U. M. Khan, *Surface Electrochemistry: A Molecular Level Approach*.New York, **1993**, p 496–500.
[39] A. J. Bard, L. R. Faulkner, *Electrochemical Methods: Fundamentals and Applications*, 2nd ed. John Wiley & Sons: New York, **2001**, p833–836.

Received: November 24, 2011
Revised: March 20, 2012
Published online: June 8, 2012

